Corrosion Science 90 (2015) 54–68

Contents lists available at ScienceDirect

Corrosion Science

journal homepage: www.elsevier.com/locate/corsci

The effects of *N*-pendants and electron-rich amidine motifs in 2-(*p*-alkoxyphenyl)-2-imidazolines on mild steel corrosion in CO_2-saturated 0.5 M NaCl

Mohammad A. J. Mazumder *, Hasan A. Al-Muallem, Shaikh A. Ali

Chemistry Department, King Fahd University of Petroleum and Minerals, Dhahran 31261, Saudi Arabia

ARTICLE INFO

Article history:
Received 6 August 2014
Accepted 22 September 2014
Available online 30 September 2014

Keywords:
A. Mild steel
B. Polarization
C. Interfaces
C. Thermodynamic diagrams

ABSTRACT

A novel series of diethylenetetramine-(**I**), and tetraethylenepentamine-derived imidazolines (**II**) having p-octyloxy-, dodecyloxy and octadecyloxy-phenyl pendants as hydrophobes, have imparted very good inhibition of mild steel corrosion in CO_2–0.5 M NaCl (40 °C, 1 atm; 120 °C, 10 bar). Pendants to the ring-nitrogen of **I** and **II** showed no change in inhibition efficiencies, while the presence of electron-rich aromatic ring in conjugation with the amidine motifs and increasing hydrophobe chain lengths imparted increasing corrosion inhibition. The formation of an imidazoline film covering the metal surface is corroborated by an XPS study. The imidazolines cover the metal surface before reaching their critical molar concentrations.

1. Introduction

Imidazolines are the most extensively used inhibitors to combat CO_2 corrosion [1–6] which inflicts huge economic losses in the oil and gas industry due to damage to pipes and other plant systems [7]. The chemical architecture of an imidazoline inhibitor consists of the following: a five-membered heterocycle embedded with an electron-rich hydrophilic amidine (N=C—N) motifs, a pendant side chain containing electron-donor hydrophilic functional group(s) and a hydrophobic alkyl chain attached to the *N* terminal and *C* of the motifs, respectively (Fig. 1). The ring-nitrogens in imidazolines **A** are weakly nucleophilic but have strong amidine bases such as 1,8-diazabicyclo[5.4.0]undec-7-ene (DBU) (pK_b 1.1) and 1,5-diazabicyclo[4.3.0]non-5-ene (DBN) (pK_b 0.5) [8]. In the presence of CO_2, the bases are reported to form bicarbonate salts **B** in aqueous media [9,10]. Imidazolines on partial hydrolysis in an aqueous solution are converted into amides **C** [9]. The reaction of an amine having a pK_b of ≈4 in aqueous CO_2 solution is complex [11,12]; in addition to the formation of carbamate salts **D** and bicarbonate salt **E**, several ionic and neutral species such as HCO_3^-, CO_3^{2-}, OH^-, H_3O^+, CO_2 and H_2O are known to coexist (Fig. 1). There lies the complexity; which of the compounds (**A**–**E**) or ionic species are involved in imparting inhibitory properties? The mechanism by which an imidazoline imparts corrosion inhibition is thus indeed complex and poorly understood.

Crude oil itself is corrosive to mild steel; CO_2/H_2O, is injected into oil wells to increase production [13], has been found to be more aggressive than hydrochloric acid at the same pH [14,15]. It is not the dry CO_2, rather its aqueous solution which imparts corrosiveness. The enhanced corrosion is attributed to the increased cathodic reduction of the species H^+, HCO_3^- as well as H_2CO_3, all of which are involved in mobile equilibria in aqueous solution of CO_2 [16,17].

The main reactions on the surface of the metal are represented by Eqs. (1)–(5) [16–18]:

$$Fe(s) + 2H_2CO_3(aq) \rightleftharpoons Fe(HCO_3)_2(aq) + H_2(g) \quad (1)$$

$$Fe(s) + 2H^+(aq) \rightleftharpoons Fe^{2+}(aq) + H_2(g) \quad (2)$$

$$Fe^{2+}(aq) + 2H_2O \rightleftharpoons Fe(OH)_2(s) + 2H^+(aq) \quad (3)$$

$$Fe(OH)_2(s) \rightleftharpoons FeO(s) + H_2O \quad (4)$$

$$Fe(HCO_3)_2(aq) \rightleftharpoons FeCO_3(s) + H_2CO_3(aq) \quad (5)$$

A coating of iron (II) carbonate on the metal surface is beneficial as it can minimize the rate of the corrosion process [19]. The solubility of iron (II) carbonate increases with increase in temperature while it dissolves at a lower pH values. Corrosion inhibitors, especially organic compounds containing electron-rich hetero-atoms and alkyl chain hydrophobes are used [20] to minimize mild steel corrosion. The inhibitor molecules may undergo physi- and/or chemisorption and form hydrophobic barrier film to shield the hydrophobes from the hostile corrosive media [21].

* Corresponding author. Tel.: +966 13 860 7836; fax: +966 13 860 4277.
E-mail address: jafar@kfupm.edu.sa (M.A.J. Mazumder).
URL: http://faculty.kfupm.edu.sa/CHEM/jafar/ (M.A.J. Mazumder).

http://dx.doi.org/10.1016/j.corsci.2014.09.014
0010-938X/

The effects of hydrophilic and hydrophobic substituents of imidazolines on their inhibition efficiency (IE) has been discussed in some detail [1,22–25]. Some researchers suggest a great role by the *N*-pendant [26], while others indicate the opposite [22]. There are also contradictory reports on the importance of the length of the hydrophobic alkyl chain on corrosion inhibition [1,23]. The inhibition efficacy of the imidazolines is attributed to their formation of a chemisorbed film on the surface of iron [1,22]. The poorly understood complex mechanism of CO_2 corrosion impeded [22,27] the design of new molecular architecture as inhibitor. In this work, syntheses of a novel class of imidazolines from *p*-alkoxybenzonitrile and oligoamines $H_2N(CH_2CH_2NH)_n$-H (n = 2 and 4) are outlined in Fig. 2. An electron-rich *p*-alkoxyphenyl substituent at the *C* is expected to augment the electron-donor capacity of the N=C—N motifs (e.g. **8**, Fig. 2); as such, one of the objectives is to examine the effect of increasing electron density of the ring-nitrogens on their inhibition efficacies. The alkoxy groups of C_8, C_{12} and C_{18} alkyl chains are intended to demonstrate the importance of hydrophobe chain length on the inhibition of CO_2 corrosion. Note that the *N*-pendants of $CH_2CH_2NH_2$ and $(CH_2CH_2NH)_2CH_2CH_2NH_2$ would allow us to compare their role to suppress corrosion of mild steel in CO_2/0.5 M NaCl solutions. We anticipate an interesting outcome of the current corrosion inhibition study aided by potentiodynamic polarizations, gravimetric weight loss, surface tension and X-ray photoelectron spectroscopy (XPS) which would improve our current understanding of the inhibition mechanism.

2. Experimental

2.1. Materials

Diethylenetetramine (DETA) (99.5%) and tetraethylenepentamine (TEPA) (~60% purity) were obtained from Aldrich Chemicals. TEPA was purified as described before [6]. *p*-Hydroxybenzoic acid, cysteine hydrochloride, bromoalkane and $SOCl_2$ from Fluka Ag (Buchs, Switzerland) were used as received. All solvents were of reagent grade.

2.2. Physical methods

IR spectra were recorded on a Perkin Elmer 16F PC FTIR spectrometer, and ^1H and ^{13}C NMR spectra were measured in $CDCl_3$ using TMS as the internal standard on a JEOL LA 500 MHz NMR spectrometer. Elemental compositions were determined with an Elemental Analyzer (Carlo-Erba: Model 1106). The digital melting point apparatus (Electrochemical-IA9100) was used to measure the melting points of all synthesized compounds. All the reactions were carried out under N_2.

2.3. Synthesis

2.3.1. General procedure for the preparation of alkyloxybenzoic acids **(3)**

The detailed procedure for the synthesis of alkoxybenzoic acid **3** is given in the supplementary materials.

2.3.2. General procedure for the synthesis of alkoxybenzamides **(4)**

The detailed procedure for the synthesis of alkoxybenzamide **4** is given in the supplementary materials.

2.3.3. General procedure for the synthesis of alkoxybenzonitriles (**5**)

The detailed procedure for the synthesis of alkoxybenzonitrile **5** is given in the supplementary materials.

2.3.4. General procedure for the synthesis of 1-(2-aminoethyl)-2-alkoxyphenyl)-2-imidazolines **(8)**

A solution of alkoxybenzonitrile **5** (25 mmol) and diethylenetriamine **6** (DETA) (62 mmol) containing cystein-HCl (100 mg) was heated at 145 °C for 1 h. Thereafter, another portion of cysteine-HCl (100 mg) was added and the reaction mixture was heated at 145 °C for an additional 1 h. Evolution of NH_3 gas was observed which bubbled through the connected U-tube containing mineral oil. ^1H NMR indicated the completion of the reaction. The reaction mixture was cooled and taken up in CH_2Cl_2 (50 cm^3). The unreacted DETA was removed from the organic layer by washing with water (3 × 300 cm^3); very careful agitation was required to avoid emulsion formation. Concentration of the dried (Na_2SO_4) organic layer afforded the imidazolines **8** as a pinkish liquid/semisolid. The imidazolines were pure as indicated by NMR spectra, and used as such for the corrosion inhibition efficiency tests. The newly synthesized imidazolines gave satisfactory elemental analyses given the fact these compounds cannot be further purified by crystallization. See supplementary materials for a detailed characterization of the imidazolines **8a**–**8c**.

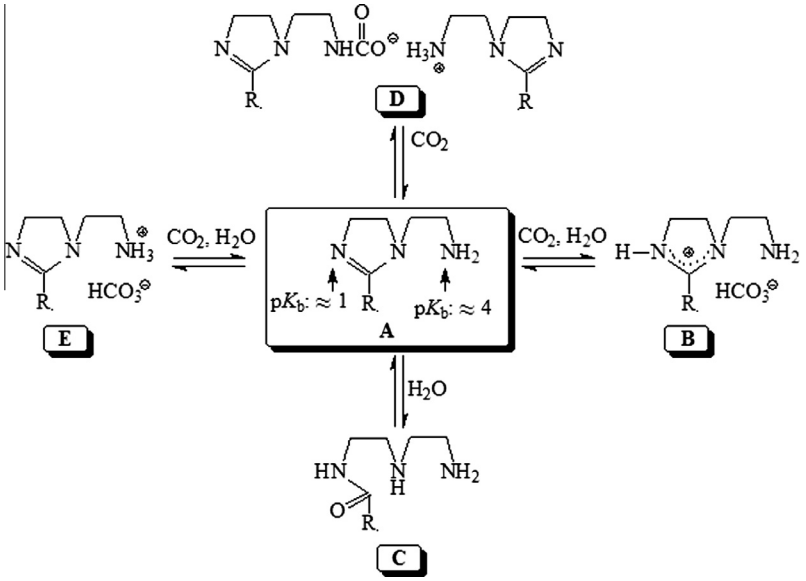

Fig. 1. Reactions of imidazolines in aqueous CO_2 solution.

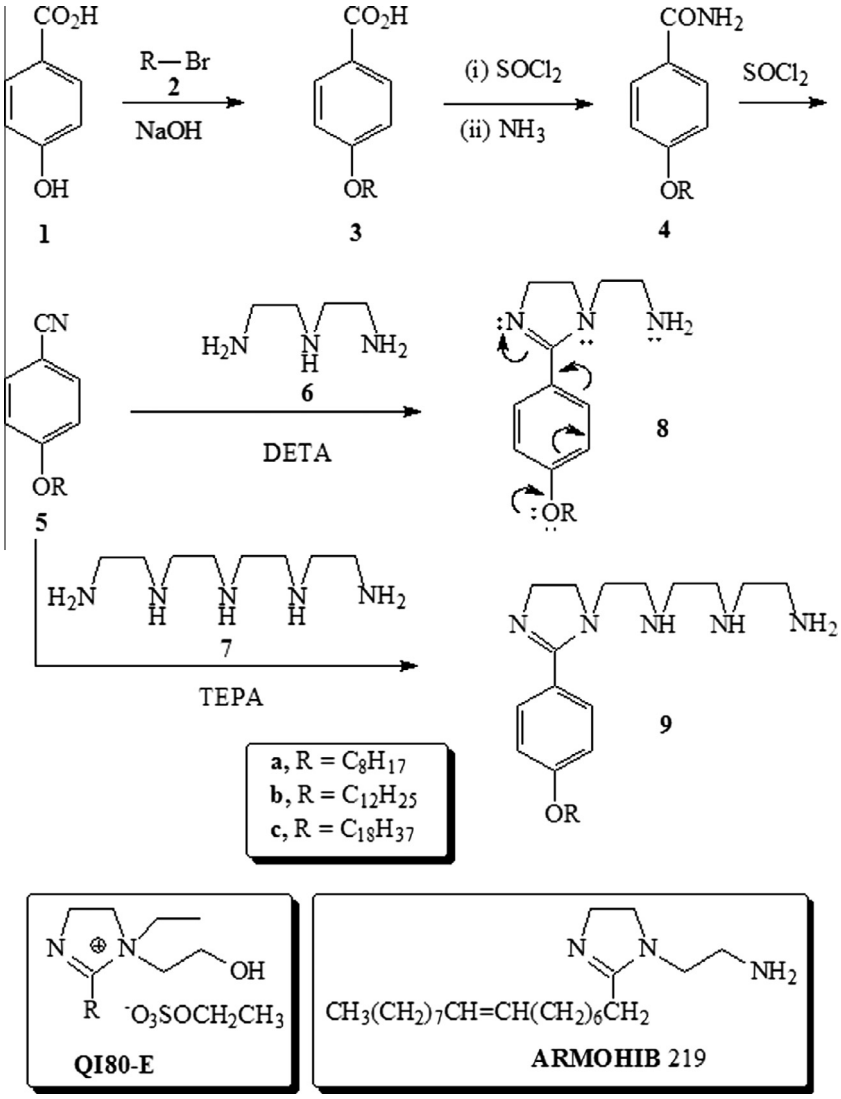

Fig. 2. Synthesis of imidazolines.

*2.3.5. General procedure for the synthesis of 1-[2-{2-(2-Aminoethylamino)-ethylamino}ethyl]-2-alkoxyphenyl-2-imidazolines **(9)***

A solution of mono- alkoxybenzonitriles **5** (25 mmol) and tetraethylenepentamine **7** (TEPA) (62 mmol) containing cysteine-HCl (100 mg) was heated at 145 °C for 1 h. Thereafter, another portion of cysteine-HCl (100 mg) was added and the reaction mixture was heated at 145 °C for an additional 1 h. Evolution of NH_3 gas was observed which bubbled through the connected U-tube containing mineral oil. ^{1}H NMR indicated the completion of the reaction. The reaction mixture was cooled and taken up in CH_2Cl_2 (50 cm^3). Similar workup as described above under Section 2.3.4 afforded the imidazolines **9** as a pinkish liquid/semisolid. The imidazolines were pure enough as indicated by NMR spectra and used as such for the corrosion inhibition efficiency tests. The detailed characterization of the imidazolines **9a**–**9c** is given in the supplementary materials.

2.4. Specimens

For the electrochemical tests, a corrosion study was carried out with mild steel coupons of the following composition (in wt%): 0.089% (C), 0.037 (Cr), 0.34% (Mn), 0.022 (Ni), 0.010 (P), 0.007 (Mo), 0.005 (V), 0.005 (Cu), 99.47% (Fe). A 1 mm thick mild steel sheet was machined to a flag shape with an approximate stem of 3 cm. Insulating the stem by Araldite (affixing material) provided 2 cm^2 exposed area which was abraded with increasing grades of emery papers (100, 400, 600 and 1500 grit size), washed with distilled deionized water and acetone, followed by oven drying at 110 °C. The dried specimens were stored in a desiccator. Before use, the electrode specimens were placed in an ultrasonic bath for 5 min, washed with distilled water and used immediately.

For autoclave tests, the two types of mild steel coupons **A** and **B** measuring ≈2.5 × 2.0 × 0.1 cm^3 have the following composition (in wt%):

Coupon A: 0.082% (C), 0.016% (Cr), 0.207% (Mn), 0.062% (Ni), 0.029% (Cu), 0.012% (Mo), <0.001% (V), 0.032% (Si), <0.0005% (P), 0.0059% (S), 0.011% (Co), 0.045% (Al), <0.0010 (Nb), <0.0005% (Ti), <99.3% (Fe).
Coupon B: 0.168% (C), 0.038% (Cr), 0.495% (Mn), 0.034% (Ni), 0.074% (Cu), 0.0081% (Mo), 0.001% (V), 0.237% (Si), 0.014% (P), 0.024% (S), 0.011% (Co), 0.080% (Al), 0.0019 (Nb), 0.0015% (Ti), <98.6% (Fe).

2.5. Solutions

Corrosion inhibition tests have been performed in 0.5 M NaCl in the presence of CO_2 (1 atm) at 40 °C as well as at higher pressure

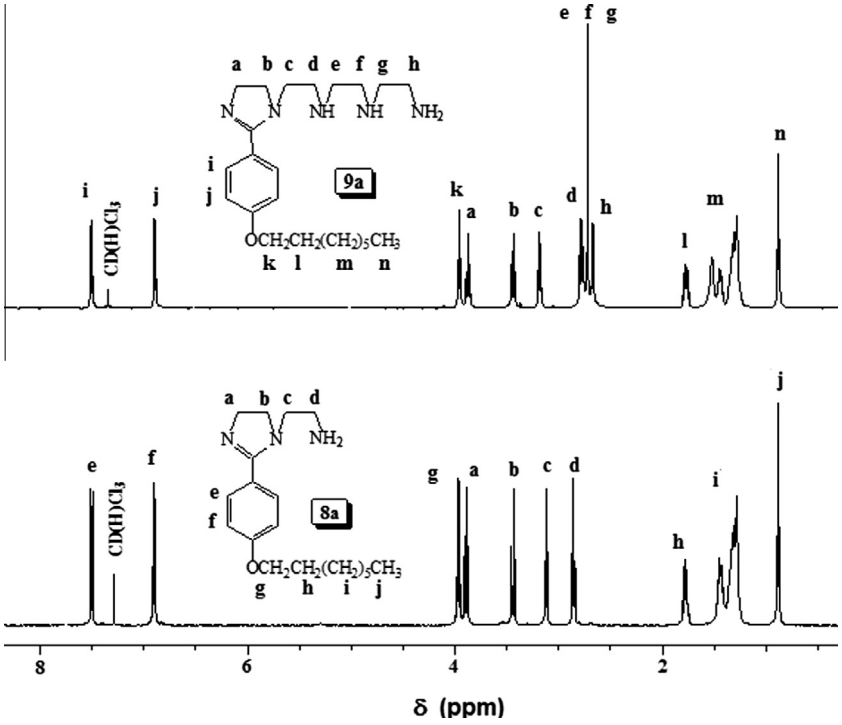

Fig. 3. ^{1}H NMR spectra of the imidazolines **8a** and **9a** in $CDCl_3$.

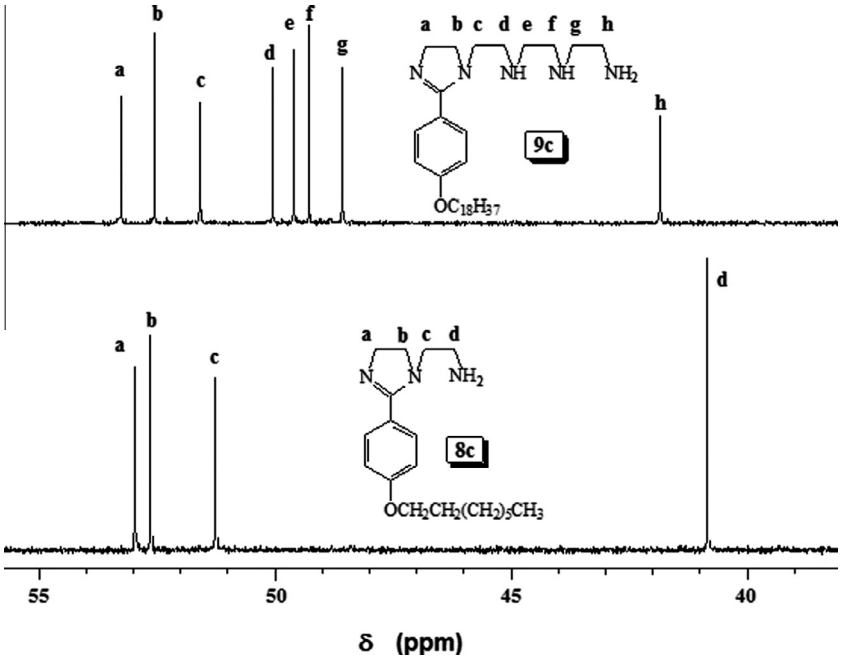

Fig. 4. ^{13}C NMR spectra of the imidazolines **8c** and **9c** in the δ 40–55 ppm range in $CDCl_3$.

(10 bar) of CO_2 and temperature of 120 °C. De-aeration of the solution was achieved by purging with 99.999% N_2 (30 min) and then the solution was saturated by continuously bubbling with 99.999% pure CO_2. During polarization measurements, instead of bubbling, the gentle flow of CO_2 was maintained above the surface of the solution without agitating the bulk of the solution. The corrosion caused by oxygen is avoided by the use of the high purity CO_2. In an aqueous solution of CO_2, at pH < 4 the corrosion usually occurs by reaction with H^+ while above pH 4 the active species is adsorbed CO_2 or H_2CO_3 [28]. In order to avoid any change in the corrosion mechanism, a solution of $NaHCO_3$ (100 mg/L) was used to maintain the pH between 5.0 and 5.5.

2.6. Electrochemical measurements

2.6.1. Tafel extrapolations

The polarization studies were carried out in a 250 cm^3 of 0.5 M NaCl solution in the presence of CO_2 (1 atm) in the absence and

Table 1
Results of Tafel plots of a mild steel sample in various solutions containing inhibitors[c] **8a–8c** in 0.5 M NaCl saturated with CO_2 at various temperatures.

Sample	Temp (°C)	Conc. (ppm)	Tafel plots				
			E_{corr} versus *SCE* (mV)	β_a (mV/dec)	β_C (mV/dec)	i_{corr} (μA/cm^2)	η (%)[a]
Blank[b]	40	0	−700	41.2	−258	103.6	–
8a	40	1	−694	75.2	−141	49.9	51.8
		5	−683	40.0	−166	38.5	62.8
		10	−677	44.3	−172	30.9	70.1
		20	−671	63.9	−181	24.6	76.2
		50	−667	45.6	−139	17.3	83.3
		100	−665	36.4	−123	8.32	92.0
8b	40	1	−691	25.0	−113	51.1	50.7
		5	−674	30.9	−128	36.9	64.4
		10	−664	23.1	−120	26.9	74.0
		20	−655	28.9	−136	19.7	80.9
		50	−646	25.4	−115	9.68	90.6
		100	−619	33.1	−127	7.55	92.7
8c	30	0	−692	46.2	−137	93.4	–
		1	−686	26.1	−119	43.1	53.8
		2	−677	33.2	−148	39.1	58.1
		3	−663	28.8	−142	36.0	61.4
		5	−656	25.7	−156	26.7	71.4
		10	−651	41.3	−149	21.6	76.8
		20	−630	30.8	−126	8.9	90.4
	40	1	−683	25.5	−114	43.1	58.4
		5	−672	34.3	−117	28.3	72.7
		10	−659	47.1	−187	20.8	79.9
		20	−651	51.4	−157	8.69	91.6
		50	−636	39.2	−148	4.81	95.4
		100	−620	43.8	−167	1.97	98.1
	50	0	−743	39.2	−157	124.1	–
		1	−728	47.1	−128	65.2	47.5
		2	−716	38.5	−146	61.1	50.7
		3	−700	24.8	−162	56.7	54.2
		5	−689	32.3	−125	39.2	68.3
		10	−681	29.4	−149	31.6	74.5
		20	−663	37.7	−153	16.3	86.8

[a] Inhibition efficiency, IE (i.e., η) = surface coverage θ.
[b] The blank was a 0.5 M NaCl solution saturated with CO_2.
[c] Inhibitor sample was dissolve in 0.5 cm^3 2-propanol, and added with 249.5 cm^3 blank solution.

presence of various concentration of inhibitors at 40 °C. The electrochemical cell, assembled in a 750 cm^3 round-bottom flask, consisted of a saturated calomel electrode (SCE) as a reference electrode, mild steel working electrode, and the graphite electrode (≈5 mm diameter) as a counter electrode. The Bubbler has one outlet and inlet for the CO_2. The polarization curves were recorded by a computer controlled potentiostat–galvanostat (Auto Lab, Booster 10A-BST707A, Eco Chemie, Netherlands). A computer (Windows 7) loaded with NOVA (Version 1.8) software processed the data. All three electrode cells were connected to the potentiostat (Auto Lab), and used for measurements. A stable open circuit potential was achieved after pre-corroding the working electrode in the solution for a certain period of time; it usually requires 30–60 min. A scan of ±250 mV with respect to the open circuit potential E_{corr} is conducted at a rate of 0.5 mV/s.

2.6.2. Linear Polarization Resistance (LPR) method

The cell described above was also used for the LPR measurement. The current potential plots (in a range of ±10 mV around E_{corr}) provided the polarization resistance values.

2.7. Gravimetric measurements at high temperature and pressure: autoclave experiments

The weight-loss measurements at a high temperature of 120 °C and a CO_2 pressure of 10 bar in a 0.5 M NaCl solution (250 cm^3) in the absence and presence of inhibitors (200 ppm) was carried out in a R&D Autoclave Bolted Closure System (Autoclave Engineers, Model # 401C-0679) for 48 h. The detailed experimental procedure is described in our earlier work [29]. The carbon-steel coupons prepared as described (*vide supra*) were immersed into the test solution.

2.8. Measurement of surface tension

The surface tension of the imidazoline samples in 0.5 M NaCl solution at 40 °C were measured by PHYWE surface tensiometer (Germany) following the operating principle of the du Nouy ring method. The surface tensiometer is equipped with torsion dynamometer (0.01 N) and platinum iridium ring with a diameter of 1.88 cm was used to measure the tear off force. Solutions of different concentrations were prepared from 0.5 M NaCl and equilibrated to 40 °C. Solutions of CO_2 saturated 0.5 M NaCl was made by passing CO_2 gas at 40 °C.

2.9. The standard free energy of micelle formation (ΔG^o_{mic})

The ΔG^o_{mic} of the synthesized imidazoline surfactant is given by Eq. (6) [30],

$$\Delta G^o_{mic} = RT \ln(C_{cmc}) \quad (6)$$

where R, T and C_{cmc} represent the gas constant, temperature and concentration in mol L^{-1} of the surfactant at the critical micelle concentration (CMC).

Table 2
Results of Tafel plots of a mild steel sample in various solutions containing inhibitors[c] **9a–9c** in 0.5 M NaCl saturated with CO_2 at various temperatures.

Sample	Temp (°C)	Conc. (ppm)	Tafel plots				
			E_{corr} versus *SCE* (mV)	β_a (mV/dec)	β_C (mV/dec)	i_{corr} (μA/cm^2)	η (%)[a]
Blank[b]	40	0	−700	41.2	−258	103.6	–
9a	40	1	−671	61.1	−249	49.2	52.5
		5	−660	32.4	−146	41.2	60.3
		10	−648	57.5	−228	29.1	71.9
		20	−645	35.8	−183	22.5	78.2
		50	−641	69.2	−124	19.6	81.1
		100	−637	66.7	−238	9.2	91.1
9b	40	1	−662	38.1	−204	47.2	54.4
		5	−643	47.2	−260	32.7	68.4
		10	−633	35.2	−168	26.4	74.5
		20	−625	56.2	−154	19.5	81.2
		50	−609	45.9	−197	14.1	86.5
		100	−605	41.8	−191	6.35	93.8
9c	30	0	−692	46.2	−137	93.4	–
		1	−683	29.8	−125	42.8	54.1
		2	−674	42.7	−156	35.2	62.4
		3	−659	38.5	−129	28.7	69.3
		5	−654	42.1	−148	20.0	78.5
		10	−633	33.0	−134	14.2	84.8
		20	−615	36.5	−149	4.13	95.6
	40	1	−668	54.5	−235	45.3	56.3
		5	−657	73.1	−194	26.1	74.8
		10	−645	87.2	−293	20.8	79.9
		20	−619	34.6	−148	6.91	93.3
		50	−598	37.6	−176	2.82	97.2
		100	−590	40.6	−212	1.97	98.1
	50	0	−743	39.2	−157	124.1	–
		1	−711	52.1	−153	62.6	49.5
		2	−694	39.4	−139	57.8	53.4
		3	−671	42.6	−116	44.9	63.8
		5	−660	29.3	−152	36.2	70.8
		10	−638	38.0	−134	28.6	76.9
		20	−626	31.9	−148	11.4	90.7

[a] Inhibition efficiency, IE (i.e., η) = surface coverage θ.
[b] The blank was a 0.5 M NaCl solution saturated with CO_2.
[c] Inhibitor sample was dissolve in 0.5 cm^3 2-propanol, and added with 249.5 cm^3 blank solution.

2.10. X-ray photoelectron spectroscopy

The metal coupons of dimension of 2.5 × 2.0 × 0.1 cm^3 as treated in electrochemical tests in CO_2 saturated 0.5 M NaCl at 40 °C for 6 h were rinsed with distilled deionized water and dried under N_2. The XPS analysis, using Advantage software for all data processing, was performed using a Thermos Scientific X-ray photoelectron spectrometer (Model # Escalab 250 Xi) and the samples were irradiated with monochromated Al K_α X-rays (1486.6 eV) of spot size of diameter 650 μm. The spectra were referenced with C 1s peak at 285.4 eV. XPS spectra were deconvoluted using a non-linear least squares algorithm with a Shirley base line and a Gaussian–Lorentzian combination.

3. Results

3.1. Synthesis of the corrosion inhibitors

As outlined in Fig. 2, the *p*-hydroxybenzoic acid **1** was O-alkylated to give *p*-alkoxycarboxylic acids **3** in very good yields. A mixture of an equimolar amount of the acid **3** and DETA **6** was heated at temperatures 185–250 °C using procedure as described [31,32] to generate the imidazolines **8**. However, a complicated mixture of products that contained variable amounts of the unreacted acid and amide along with the desired imidazoline **8** (≈50%) was obtained. This mixture may as well serve as an effective inhibitor mixture. However, our objective was to synthesize and determine the inhibition efficiencies of the pure imidazolines alone. To pursue the synthesis of the proposed imidazolines, we designed a different synthetic protocol; the use of nitrile (CN) instead of acid (CO_2H) group was envisaged. For this purpose, nitriles **5** have been prepared in very good yields as illustrated in Fig. 2. Here again we encountered difficulties; the reaction of the nitrile **5** with DETA **6** using procedure as mentioned in a patent [33] using CS_2 as a catalyst failed to give the imidazoline **8** in the temperature range 110–145 °C. However, to our delight, changing the catalyst to cysteine. HCl and temperature at 145 °C led to the formation of the imidazolines **8** and **9** using DETA **6** and TEPA **7**, respectively, in very good yields. The imidazolines were readily identified by ^{1}H and ^{13}C NMR spectroscopy. The ^{1}H NMR spectra of the imidazolines **8a** and **9a** and ^{13}C NMR spectra of **8c** and **9c** are shown in Figs. 3 and 4, respectively. The carbon spectra revealed the presence of four and eight signals for the carbon marked as **a–d** and **a–h** in **8c** and **9c**, respectively. Note that our synthetic objective is achieved by having a series of imidazolines bearing different *N*-substituents and alkoxy chains in order to assess and compare their inhibition effects.

Two commercial inhibitor samples: **QI80-E** (R = C_{12} to C_{22}) from Materials Performance and **ARMOHIB 219** from AKZO NOBEL are also tested for the purpose of comparison (Fig. 2).

3.2. Electrochemical measurements

3.2.1. Tafel extrapolation

The corrosion inhibition results of inhibitors **8a–c** and **9a–c**, carried out in a CO_2-saturated 0.5 M NaCl solution using Tafel plot

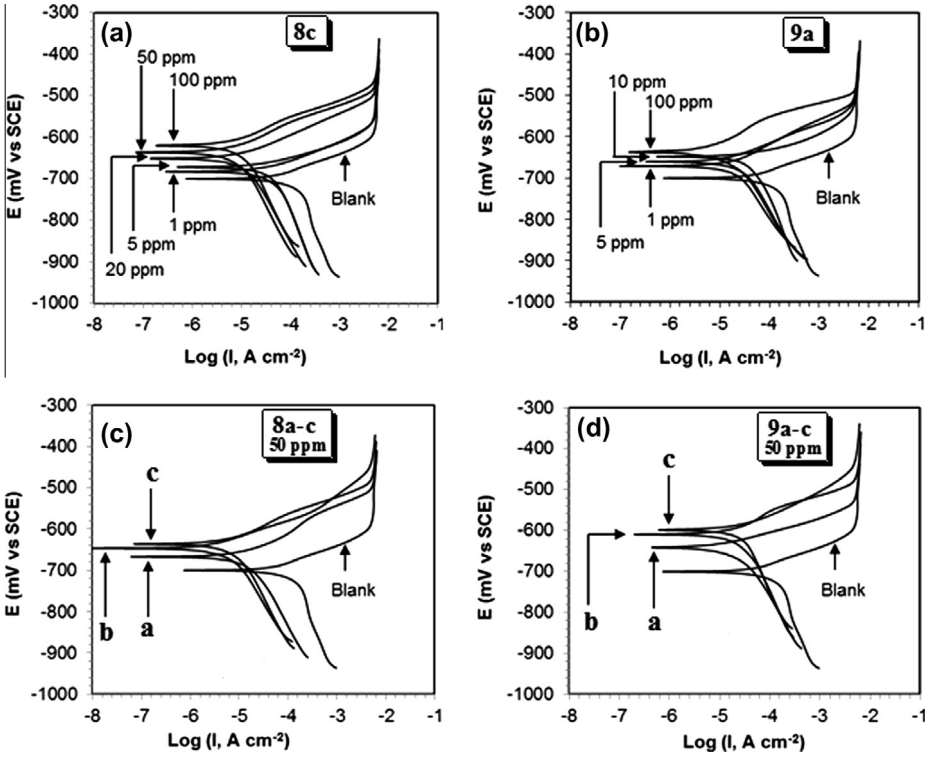

Fig. 5. Potentiodynamic polarization curves at 40 °C for mild steel in CO_2 saturated 0.5 M NaCl containing various concentrations of (**a**) **8c**, (**b**) **9a**, and 50 ppm of (**c**) **8** and (**d**) **9**.

extrapolation, are summarized in Tables 1 and 2. The pH was kept in the range of 5.0–5.5 to minimize direct reduction of H_2CO_3 (Eq. (1)) [34,35]. Some representative Tafel plots are shown in Fig. 5. Each pair of Tafel plots was analyzed [36] to obtain the corrosion current density (i_{corr}) and the corrosion potential (E_{corr}). The extrapolation of cathodic Tafel lines with respect to free corrosion potential from Tafel plots was determined by using a computer (Windows 7) controlled potentiostat–galvanostat (AutoLab, Eco Chemie, Netherlands) instrument with a utilization of automated linear curve fitting Nova 1.8 software.

3.2.2. LPR

The η% from LPR technique was calculated using Eq. (7):

$$\eta(\%) = \left(\frac{R'_p - R_p}{R'_p}\right) \times 100 \tag{7}$$

where R_p and R'_p are the respective polarization resistances in solution without or with the inhibitors in CO_2-saturated 0.5 M NaCl at 40 °C (Tables 3 and 4). The tables also include some inhibition data obtained at 30 °C and 50 °C. The results of Tafel extrapolation and LPR at 40 °C are compared in Table 5.

3.3. Adsorption isotherms

Fractional inhibition efficiency η, equated to surface coverage θ of the electrode by an inhibitor molecule at its lower concentration range, is reported in the Tables 1–4. Note that at higher inhibitor concentrations η versus θ relationship does not remain linear owing to a transition from a monolayer to a multilayer coverage. The θ values obtained by LPR method (Tables 3 and 4) in CO_2-saturated 0.5 M NaCl and C (the concentration in mol L^{-1}) were used to find the best among the following adsorption isotherms, namely:

Temkin:

$$K_{ads}C = e^{f\theta} \tag{8}$$

Langmuir:

$$\theta/(1-\theta) = K_{ads}C \tag{9}$$

Frumkin [37]:

$$K_{ads}C = \{\theta/(1-\theta)\}e^{-2a\theta} \tag{10}$$

Freundluich [38]:

$$\theta = K_{ads}C^n \tag{11}$$

where K_{ads} is the equilibrium constant of the adsorption process. The correlation coefficient revealed the best fit for the Langmuir isotherm for the inhibitors in CO_2 saturated 0.5 M NaCl (Fig. 6 and Table 6). Some of the inhibitors demonstrated a good fit for both the Temkin as well as Langmuir adsorption isotherms. The molecular interaction parameter f, which describes molecular interactions in the adsorption layer as well as inhomogeneities on the surface of the electrode, was calculated from the Temkin isotherm (Table 6) [34,38].

The K_{ads} is related to the free energy of adsorption (ΔG^o_{ads}), by:

$$K_{ads} = \frac{1}{55.5}\exp\left(\frac{-\Delta G^\circ_{ads}}{RT}\right) \tag{12}$$

The values of K_{ads} and ΔG^o_{ads} are summarized in Table 7. The ΔS^o_{ads} and ΔH^o_{ads} for the adsorption process of the imidazolines **8c** and **9c** in the temperature range 30–50 °C was obtained from a plot of ΔG^o_{ads} versus T as shown in Fig. 7.

3.4. Gravimetric measurements in CO_2-saturated 0.5 M NaCl at high temperature and pressure

The results of the experiments carried out at a temperature of 120 °C and a pressure of 10 bar CO_2 in 0.5 M NaCl for 48 h are given in Table 8. Duplicate determinations were made in each case using coupons of almost identical masses. Percent inhibition efficiency (η%) was calculated using Eq. (13):

Table 3
Results of LPR method in 0.5 M NaCl saturated with CO_2 at various temperatures.

Sample	Temp (°C)	Concentration (ppm by weight)	Polarization resistance		
			R'_p (Ω cm^2)	θ^a	θ (%)
Blank[b]	40	0	89.7	–	–
8a	40	1	218	0.589	58.9
		5	247	0.637	63.7
		10	276	0.675	67.5
		20	340	0.736	73.6
		50	568	0.842	84.2
		100	973	0.908	90.8
8b	40	1	194	0.538	53.8
		5	290	0.691	69.1
		10	315	0.715	71.5
		20	388	0.769	76.9
		50	653	0.863	86.3
		100	1059	0.915	91.5
8c	30	0	82.3	–	–
		1	165	0.502	50.2
		2	192	0.572	57.2
		3	226	0.635	63.5
		5	301	0.726	72.6
		10	471	0.825	82.5
		20	1107	0.925	92.5
	40	1	210	0.573	57.3
		5	305	0.706	70.6
		10	477	0.812	81.2
		20	809	0.889	88.9
		50	1317	0.932	93.2
		100	1800	0.950	95.0
	50	0	97.8	–	–
		1	172	0.431	43.1
		2	196	0.500	50.0
		3	218	0.552	55.2
		5	297	0.671	67.1
		10	451	0.783	78.3
		20	689	0.858	85.8

[a] Surface coverage, θ = Inhibition Efficiency, IE (i.e., η).
[b] 0.5 M NaCl solution saturated with CO_2.

Table 4
Results of LPR method in 0.5 M NaCl saturated with CO_2 at various temperatures.

Sample	Temp (°C)	Concentration (ppm by weight)	Polarization resistance		
			R'_p (Ω cm^2)	θ^a	θ (%)
Blank[b]	40	0	89.7	–	–
9a	40	1	162	0.446	44.6
		5	214	0.581	58.1
		10	281	0.681	68.1
		20	355	0.747	74.7
		50	515	0.826	82.6
		100	918	0.902	90.2
9b	40	1	212	0.577	57.7
		5	260	0.655	65.5
		10	332	0.730	73.0
		20	509	0.824	82.4
		50	540	0.834	83.4
		100	1181	0.924	92.4
9c	30	0	82.3	–	–
		1	169	0.514	51.4
		2	213	0.613	61.3
		3	256	0.678	67.8
		5	336	0.755	75.5
		10	592	0.861	86.1
		20	2562	0.968	96.8
	40	1	176	0.493	49.3
		5	386	0.768	76.8
		10	616	0.854	85.4
		20	1019	0.912	91.2
		50	1695	0.947	94.7
		100	2045	0.956	95.6
	50	0	97.8	–	–
		1	197	0.504	50.4
		2	225	0.565	56.5
		3	274	0.643	64.3
		5	313	0.687	68.7
		10	546	0.821	82.1
		20	902	0.892	89.2

[a] Surface coverage, θ = Inhibition Efficiency, IE (i.e., η).
[b] 0.5 M NaCl solution saturated with CO_2.

$$\eta\% = \frac{\text{Weight loss(without inhibitor)} - \text{Weight loss(inhibitor)}}{\text{Weight loss(without inhibitor)}} \times 100 \quad (13)$$

Where the masses of the coupons differed, relative weight loss of the coupons were used to calculate the η% [36,39]. The average η% reported in the Table 8 is found to have a standard deviation of 2–3%.

3.5. Surface tension

The surface tension γ and critical CMC values for the imidazolines **8** and **9** are measured in 0.5 M NaCl and 0.5 M NaCl + CO_2 at 40 °C and the results are given in Table 9. Fig. 8a and b shows the plot of surface tension γ against the concentration of the imidazolines under various conditions.

3.6. X-ray photoelectron spectroscopy

The plots of the intensity (counts) versus binding energy (eV) as measured by XPS are shown in Figs. 9 and 10. The results of the surface analysis are given in Table 10.

4. Discussion

A series of novel imidazolines having variance in the pendants attached to the N and C of the functional amidine motifs (N=C–N) embedded in the five-membered imidazolines **8** and **9**. One common structural component in the current imidazolines is the strategic placement of the aromatic ring in conjugation with the N=C–N motifs. This allows the shifting of charge density from the electron-rich benzene ring to the imidazolines as shown using structure **8** (Fig. 2). This stabilizing electron movement would force the two rings to be coplanar; the electron-rich motifs N=C–N along with aromatic π-clouds are expected to undergo strong adsorption by formation of coordinate-type bonds with the empty d-orbitals of Fe on the anodic sites of the metal surface.

The highly surface-active imidazolines **8** and **9** used in this study demonstrated very good corrosion inhibition in a CO_2-saturated 0.5 M NaCl (Tables 1–5). The LPR study revealed θ% values of 73.6, 76.9, and 88.9 at a concentration of 20 ppm of the DETA-derived imidazolines **8a**, **8b** and **8c**, respectively (Table 3). For the corresponding TEPA-derived imidazolines **9a**, **9b** and **9c**, the respective θ% at 20 ppm were found to be 74.7, 82.4 and 91.2 (Table 4). At various concentrations of the inhibitors, the pentamine derivatives **9** imparted slightly better inhibition efficiencies than their triamine counterparts **8**. Note that a concentration of 20 ppm of **8a**, **8b**, **8c** and **9a**, **9b**, **9c** translates into their respective concentrations of 63.0, 53.5, 43.7, 49.6, 43.5 and 36.8 μM, respectively. Higher polyamine chain length seems to augment the corrosion inhibition to a limited extent. Both **8c** and **9c** having hydrophobic alkyl chain of C_{18} have shown better inhibition efficacies than their respective C_8 or C_{12} counterparts **8a**, **9a** and **8b**, **9b**. Increase in the θ% values with increasing alkyl chain lengths could be attributed to the extra coverage of the metal surface possible for

Table 5
Corrosion inhibition efficiency, η (%) using polarization resistance and Tafel plots of mild steel samples in various solutions containing 50 and 100 ppm by weight of the inhibitors in 0.5 M NaCl solution saturated with CO_2 (1 atm) at 40 °C.

Compound	η (%)					
	Polarization method			Tafel method		
	20[a]	50[a]	100[a]	20[a]	50[a]	100[a]
8a	73.6	84.2	90.8	76.2	83.3	92.0
8b	76.9	86.3	91.5	80.9	90.6	92.7
8c	88.9	93.2	95.0	91.6	95.4	98.1
9a	74.7	82.6	90.2	78.2	81.1	91.1
9b	82.4	83.4	92.4	81.2	86.5	93.8
9c	91.2	94.7	95.6	93.3	97.2	98.1

[a] inhibitor concentration in ppm by weight.

the longer hydrophobic tails. The results of the Tafel extrapolations (Tables 1 and 2) corroborated the findings of the LPR method (Tables 3 and 4). As evident from Table 5, at a concentration of 100 ppm, all the imidazolines imparted very good IEs, especially **8c** and **9c** – both having η% of over 98.

Fig. 5 shows the Tafel plots for the imidazolines, and their Tafel constants, corrosion potentials and IEs are included in Tables 1 and 2. The E_{corr} values in all the cases progressively shifted to less negative values (i.e. noble direction) with the increase in the inhibitor concentrations, thereby indicating that the imidazolines are suppressing mainly the anodic reactions (Fig. 5). A difference of E_{corr} values between the blank and inhibited solution (100 ppm) in the ranges of 35–72 mV (Table 1) and 57–78 mV (Table 2) for (**8a**, **8b**, **8c**) and (**9a**, **9b**, **9c**), respectively, does not qualify these inhibitors to be classified under the anodic type. Classification of a compound as a cathodic or anodic type inhibitor is feasible when the E_{corr} is shifted at least by 85 mV [40].

Inhibitor action is more pronounced in the anodic Tafel lines as the difference between anodic current densities in the absence and presence of inhibitor are much greater than the corresponding differences in the cathodic branches (Fig. 5). The inhibitors thus

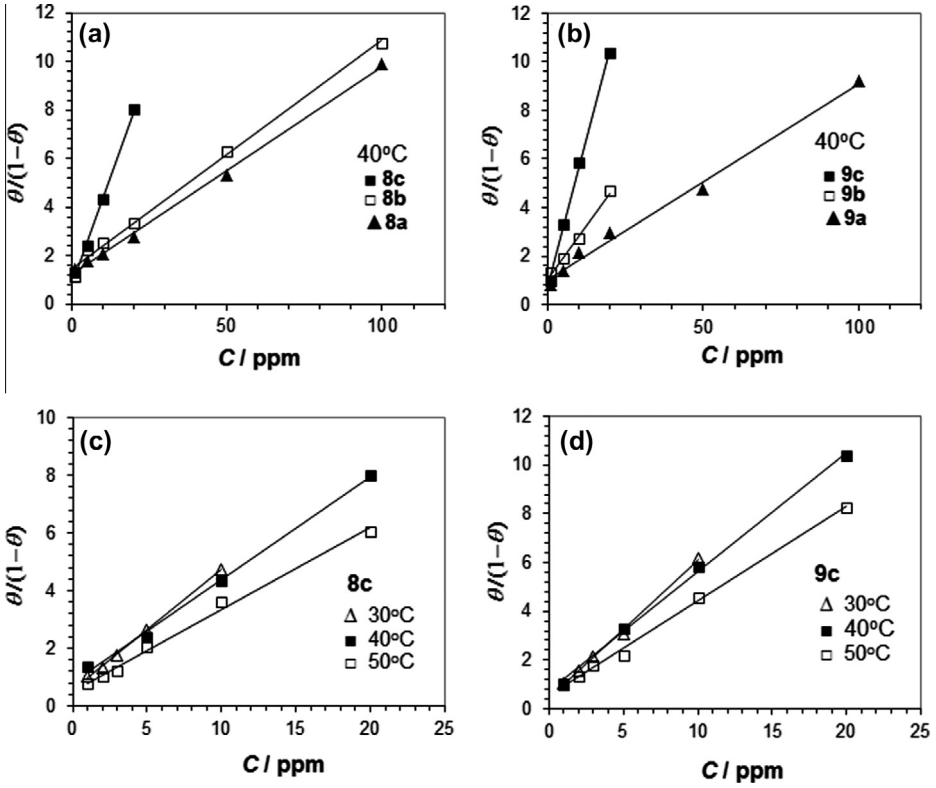

Fig. 6. Langmuir adsorption isotherm of (**a**) **8a**, **b**, **c** and (**b**) **9a**, **b**, **c** at 40 °C, (**c**) **8c** and (**d**) **9c** at various temperatures in CO_2 saturated 0.5 M NaCl solution.

Table 6
Square of coefficient of correlation (R^2) and values of the constants in the adsorption isotherms of Temkin, Frumkin, Langmuir and Freundlich in the presence of inhibitors **8** and **9** in CO_2 Saturated 0.5 M NaCl solution (LPR data used for the isotherm).

Compound	Temp (°C)	Temkin (R^2, f)	Langmuir (R^2)	Frumkin (R^2, a)	Freundlich (R^2)
8a	40	0.9260, 14	0.9984	0.7313, −3.5	0.9503
8b	40	0.9912, 12	0.9956	0.9387, −3.2	0.9843
8c	30	0.9901, 6.9	0.9992	0.8389, −1.1	0.9952
	40	0.9831, 9.4	0.9971	0.8128, −1.9	0.9929
	50	0.9848, 6.6	0.9940	0.8105, −0.85	0.9822
9a	40	0.9954, 10	0.9919	0.9542, −2.4	0.9864
9b	40	0.9338, 13	0.9936	0.7907, −3.4	0.9573
9c	30	0.9997, 6.6	0.9972	0.8551, −0.78	0.9948
	40	0.9808, 7.0	0.9968	0.9961, −0.73	0.9591
	50	0.9874, 7.4	0.9967	0.7608, −0.99	0.9881

Table 7
The values of the adsorption equilibrium constant from Langmuir adsorption isotherms and free energy, enthalpy, entropy changes of the mild steel dissolution in the presence of inhibitors **8** and **9** in CO_2 saturated 0.5 M NaCl at various temperatures.

Compound	Temp (°C)	$K_{ads} \times 10^{-5}$ (L mol^{-1})[a]	ΔG^{o}_{ads} (kJ mol^{-1})	ΔH^{o}_{ads} (kJ mol^{-1})	ΔS^{o}_{ads} (J mol^{-1} K^{-1})
8a	40	27,083	−37.0	–	–
8b	40	34,995	−37.7	–	–
8c	30	191,106	−40.8	−15.8	+82.5
	40	163,330	−41.7		
	50	129,573	−42.4		
9a	40	32,676	−37.5	–	–
9b	40	81,241	−39.9	–	–
9c	30	310,441	−42.0	−16.3	+85.0
	40	266,094	−43.0		
	50	210,417	−43.7		

[a] K_{ads} obtained in L/mg was converted to L/mol.

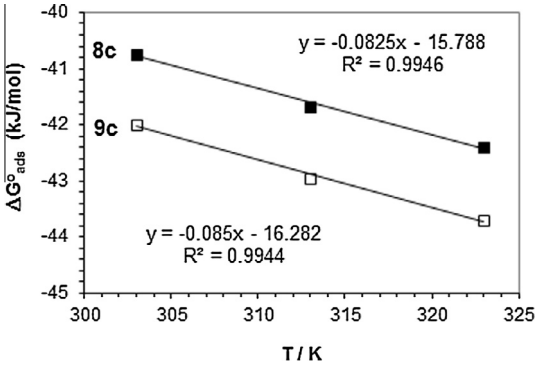

Fig. 7. Variation of ΔG^{o}_{ads} versus T on mild steel in CO_2 Saturated 0.5 M NaCl containing **8c** and **9c**.

retards the anodic dissolution of iron more than the cathodic hydrogen evolution reaction. As evident from the Tables 1 and 2, the cathodic (β_c) and anodic (β_a) slopes in most cases are not affected considerably thereby implying that the mechanism of reactions happening at the electrodes are not changed in the presence of the inhibitors. The inhibitors simply block the anodic and cathodic reaction sites. The E_{corr} shifts suggest that the studied compounds in CO_2 saturated 0.5 M NaCl solution act as mixed-type inhibitors under the predominance of anodic control. Fig. 5 shows that the shift in the anodic direction increases in the order: **8a < 8b < 8c** and **9a < 9b < 9c**, and the shift in the presence of pentaamine-derived inhibitors **9** were found to be slightly higher than those of triamine-derived imidazolines **8**. The negative values of ΔH^{o}_{ads} suggest exothermic physisorption of the inhibitors on the metal surface, while negative ΔG^{o}_{ads} certify their favorability (Table 7) [35]. The relatively smaller values of $-\Delta G^{o}_{ads}$ values in the range of 37–43 kJ/mol, which are greater than 20 kJ/mol, indicate the electrostatic (i.e. physisorption) and chemisorption adsorption mechanism of the imidazolines on mild steel [34,40]. A protective film can be constructed by the formation of a coordinate type chemical bonds between d-orbitals of iron and the non-bonding as well as π-electrons in the electron-rich imidazoline motif and the aromatic ring [41,42]. Moderate positive values for the entropy change, ΔS^{o}_{ads}, ascertain the favorable increase in the randomness as a result of displacement of water molecules from the metal surface (Table 7). Note that as the temperature increases the E_{corr} becomes more negative (less noble), which makes the metal surface more susceptible to media attack.

Some of the anodic polarization curves in the current-versus-potential plots, especially in the higher concentration range of the inhibitors, have current-increasing plateaus which are called the desorption potentials [41,43] (Fig. 5). Significant steel dissolution happens at potentials higher than the desorption potential thereby suggesting a mechanism by which the inhibitors block the anodic sites on the metal surface.

The surface coverage data (θ) indicate that the adsorption of the imidazolines are fitted best by the Langmuir adsorption isotherm; while some of them followed Temkin as well as Freundlich adsorption isotherms (Table 6). The relatively higher values of the energetic inhomogeneity factor f obtained from Temkin model signify

Table 8
Corrosion rates and inhibition efficiencies of various corrosion inhibitors (200 ppm by weight) at 120 °C and 10 bar pressure of CO_2 in 0.5 M NaCl solution.

Solution	Coupon[a]	**CR**[b] (mm y^{-1})	% Inhibition	Average % Inhibition
Blank	**A**	2.19	–	–
	B	2.23	–	
8a	**A**	0.607	72.3	71.8
	B	0.638	71.4	
8b	**A**	0.195	91.1	90.8
	B	0.212	90.5	
8c	**A**	0.149	93.2	93.1
	B	0.156	93.0	
9a	**A**	0.569	74.0	72.5
	B	0.647	71.0	
9b	**A**	0.153	93.0	92.4
	B	0.181	91.9	
9c	**A**	0.153	93.0	93.3
	B	0.143	93.6	
Q I 80	**A**	0.429	80.4	81.0
	B	0.410	81.6	
ARMOHIB29	**A**	0.396	81.9	82.7
	B	0.368	83.5	

[a] Two mild steel coupons **A** and **B** having different carbon content and compositions.
[b] Corrosion rate.

Table 9
Surface properties of imidazolines **8** and **9** in 0.5 M NaCl at 40 °C.

Compound	Surface tension (mN m^{-1})	C_{cmc} (μmol L^{-1})	C_{cmc} (ppm)	ΔG^{o}_{mic} (kJ mol^{-1})
8a	33.5	30.2	9.59	−27.1
8a[a]	35.0	37.4	11.9	−26.5
8b	31.5	21.8	8.14	−27.9
8c	29.3	20.0	9.15	−28.2
9a	36.2	22.4	8.99	−27.9
9b	34.0	18.3	8.38	−28.4
9c	31.2	13.9	7.53	−29.1

[a] 0.5 M NaCl saturated with CO_2.

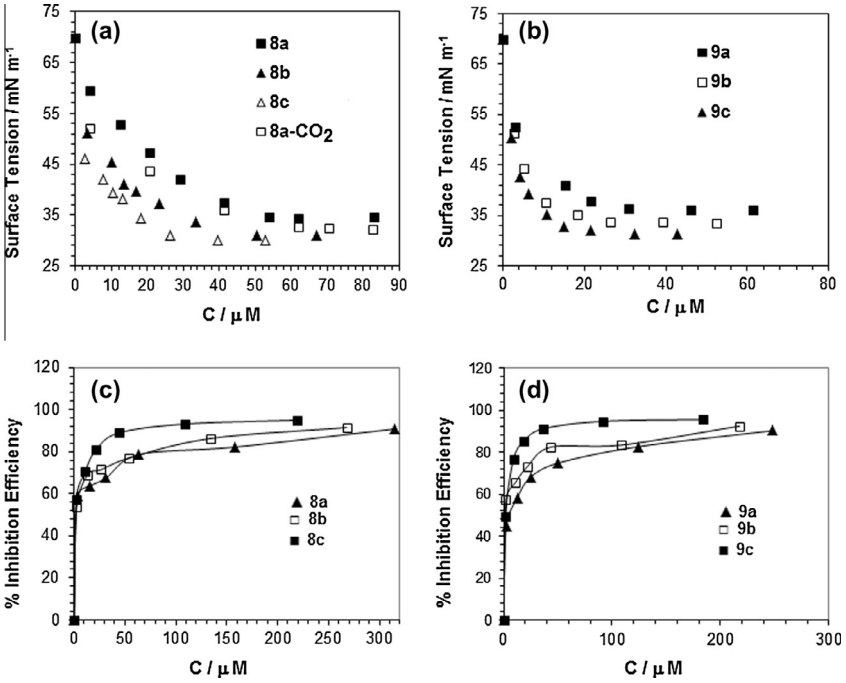

Fig. 8. Surface tension versus concentration of imidazoline (**a**) **8** and (**b**) **9** in 0.5 M NaCl solution; and inhibition efficiency versus concentration of imidazolines (**c**) **8** and (**d**) **9** in CO_2 saturated 0.5 M NaCl solution at 40 °C.

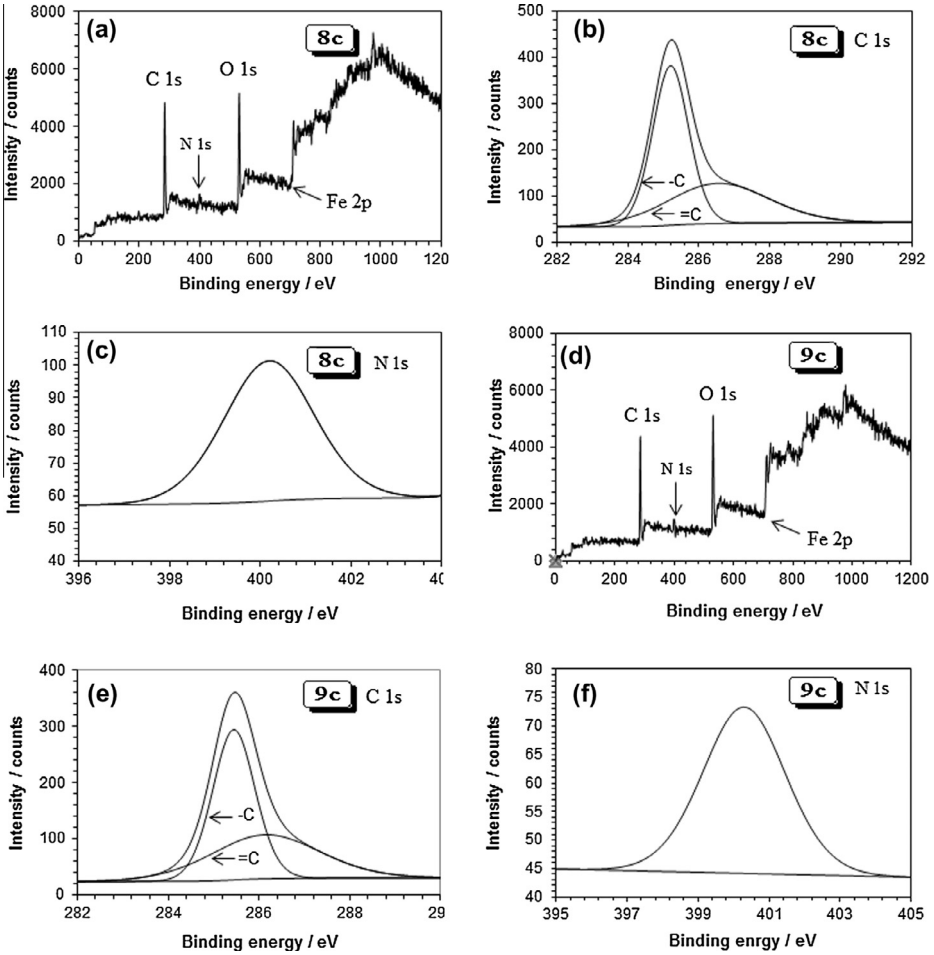

Fig. 9. (**a**) XPS spectrum of Fe and the XPS deconvoluted profiles of (**b**) C 1s and (**c**) N 1s after immersing in CO_2 saturated 0.5 M NaCl at 40 °C for 6 h in the presence of 8c (100 ppm); and (**d**) the corresponding XPS spectrum and XPS deconvoluted profiles of (**e**) C 1s and (**f**) N 1s in the presence of **9c**.

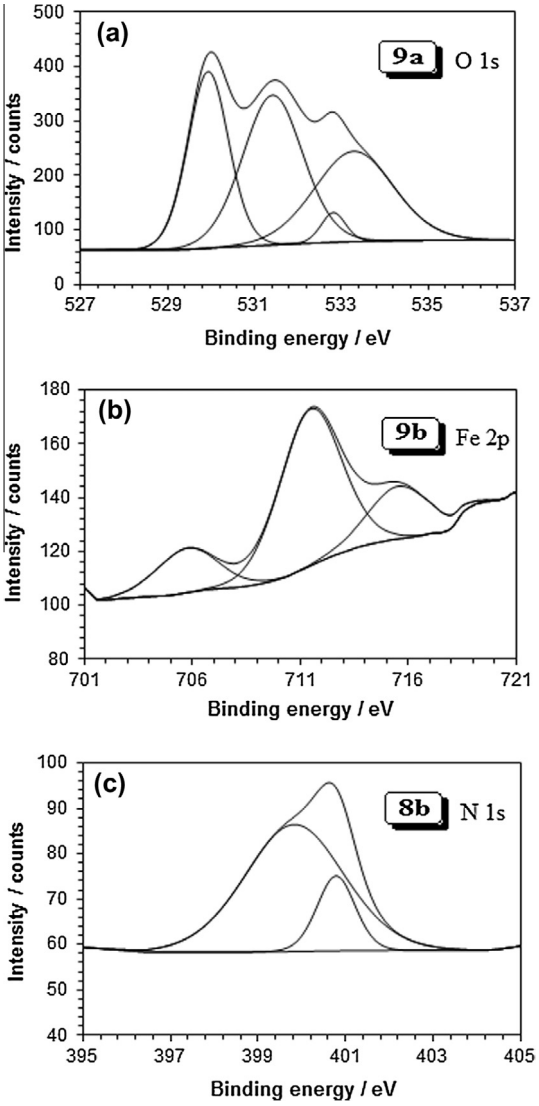

Fig. 10. XPS deconvoluted profiles of (**a**) O 1s, (**b**) Fe 2p in the presence of 100 ppm of **9a** and **9b**, respectively, (**c**) N 1s in the presence **8b** (100 ppm) after immersing Fe in CO_2 saturated 0.5 M NaCl at 40 °C for 6 h.

a strong dependence of free energy of adsorption on the surface coverage [44,45].

The imidazolines performed very well at higher temperature (120 °C) and pressure (10 bar, CO_2) to arrest corrosion in 0.5 M NaCl (Table 8). The inhibition efficacy η% of the imidazolines, as determined using two types of metal coupons **A** and **B** having different elemental compositions and carbon content, were found to increase in the following order: **8c > 8b > 8a** and **9c > 9b > 9a**. We noted, quite joyfully, that the current imidazolines having C_{12} (**8b**, **9b**) and C_{18} (**8c**, **9c**) alkyl chains, outperformed the two commercial imidazolines **QI80** and **ARMOHIB219** (Table 8).

The objective of constructing the surface tension versus inhibitor concentration profile is to find the imidazoline's CMC which can be used to compare the adsorption pattern on either side of the CMC. The imidazolines in aqueous media are classified as cationic surfactants because of the involvement of the cationic form **B** in equilibrium with its neutral counterpart **A** (Fig. 1) [46]. In terms of molar concentration, the CMC as well as surface tension of the imidazolines are found to follow the orders: **8a > 8b > 8c; 9a > 9b > 9c;** and **8 > 9** (Table 9). In the aqueous 0.5 M NaCl solution, the pentamine derivatives **9**, having greater hydrophilic polar heads, are expected to have greater CMC values for being more soluble in water than its triamine counterparts. However, we cannot offer a rationale for the opposite finding. The increase in the hydrophobic alkyl chain length decreases the solubility of the imidazolines, and as expected decreases the CMC [47]. The C_{18} alkyl tails by virtue of having the greater hydrophobic interactions leads to a smaller CMC values for the imidazolines **8c** and **9c**. Note that imidazoline **8a** in CO_2 saturated 0.5 M NaCl has a CMC value of 37.4 μM (≈11.9 ppm), whereas in the absence of CO_2 it becomes 30.2 μM (≈9.59 ppm). The formation of carbamate salt of imidazoline in CO_2 saturated NaCl solution makes it more water-soluble hence increases the CMC value (*vide infra*). A closer look at the CMC values (Figs. 8a,b and Table 9) and the surface coverage (θ) data (Fig. 8c,d, and Tables 3 and 4) reveals that imidazolines cover most of the surface before the concentrations reach their CMC values. The adsorption on the metal surface is favored over the micellization since the ΔG^{o}_{ads} values are more negative (Table 7) compared with the corresponding ΔG^{o}_{mic} (Table 9). The monolayer formation at the interface between the metal and solution is complete before the CMC, after which multilayer coverage as a result of adsorption of the micelles may impart further protection, albeit to a lesser degree [48].

Table 10
XPS survey scan composition of Fe immersed in inhibited solution of 0.5 M NaCl–CO_2 (1 atm) at 40 °C for 4 h.

Peak	Approx. binding energy (eV)	Composition (atom%)					
		8a	**8b**	**8c**	**9a**	**9b**	**9c**
C 1s	285.4	24.6	30.8	34.9	28.7	45.0	32.3
C 1s	286.4	37.8	32.7	24.8	22.8	19.1	24.3
O 1s	530.1	9.0	9.0	4.0	11.5	4.5	11.5
O 1s	531.5			26.5	14.4	1.6	5.7
O 1s	532.9	19.4	19.2		1.2	23	16.9
O1s	534.4	9.5			11.4		
N 1s	400.0		4.7	5.2	5.0		
N 1s	400.6	3.3	1.1			4.4	5.5
Fe 2p	706.3		0.2			0.4	
Fe 2p	711.0	1.4	1.9	2.3	4.2	1.5	3.3
Fe 2p	714.3	0.78	0.4	0.6	0.8	0.5	0.5
Cl 2p	197.55 199.19	0.92		1.7			

The XPS survey scan composition of Fe immersed in an inhibited solution of 0.5 M NaCl–CO_2 revealed the presence of a carbonaceous film on the metal surface as indicated by its high carbon and small Fe contents (Table 10). The presence of N points (Figs. 9c,f and 10c) its origin to the imidazolines; the metal surface is thus covered by a film of imidazolines. The XPS spectra, for instance, in the presence of inhibitors **8c** and **9c** are shown in Fig. 9a and d, respectively.

The XPS deconvoluted profiles of C 1s spectrum for **8c** and **9c** revealed a two-peak profile (Fig. 9b and e); the peak at 285.4 eV was assigned to the C—C aliphatic bonds, while the presence of C═C, C═O, and C—N bonds were reflected by the peak at 286.4 eV. The presence of O 1s peaks at 530.1 and 531.5 eV is attributed to the O^{2-} in Fe_2O_3 and hydrous iron oxide FeOOH, respectively (Fig. 10a) [49,50]. The other O 1s peaks at 532.9 and 534.3 may be associated with the oxygen of adsorbed water. Small intensity peaks at 711 and 706.3 are indicative of the presence of Fe^{3+} (2p) and Fe^{0} (2p) (Fig. 10b). The peak located around 714.3 is indicative of the presence of a small concentration of $FeCl_3$.

Imidazolines **8b** and **9b** (both having hydrophobe length equivalent to 17 CC bonds) at a concentrations of 1, 5 and 10 ppm are found to impart better corrosion protection than their corresponding imidazolines having heptadecyl (C_{17}) alkyl chains **10** and **11**, respectively (Fig. 11). The length of the benzene ring is considered as equivalent to four CC bonds and O is assumed to be an

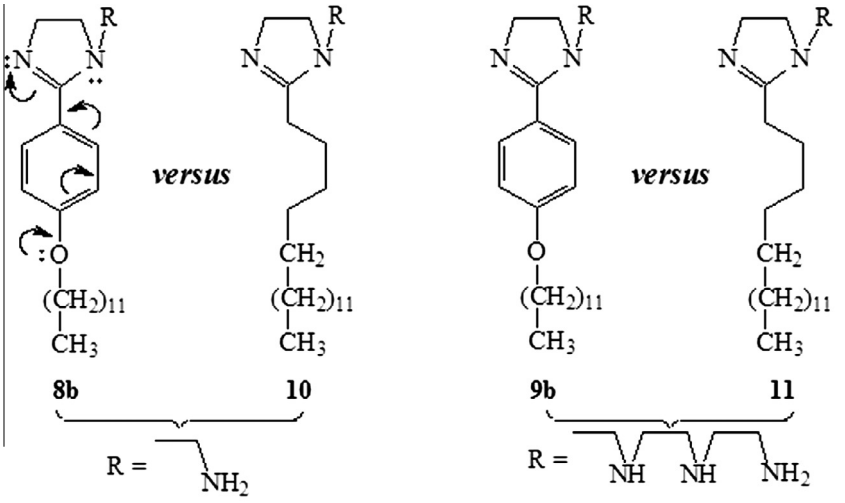

Imidazoline	η % at concentration (ppm) of 1	5	10	20	50
8b	53.8	69.1	71.5	76.9	86.3
10	23.1	54.0	64.7	-	84.5
9b	57.7	65.5	73.0	82.4	83.4
11	<14.3	<49.9	65.4	87.2	90.2

Fig. 11. Comparative inhibition behavior of imidazolines having similar pendant chain length: **8b** versus **10** and **9b** versus **11**.

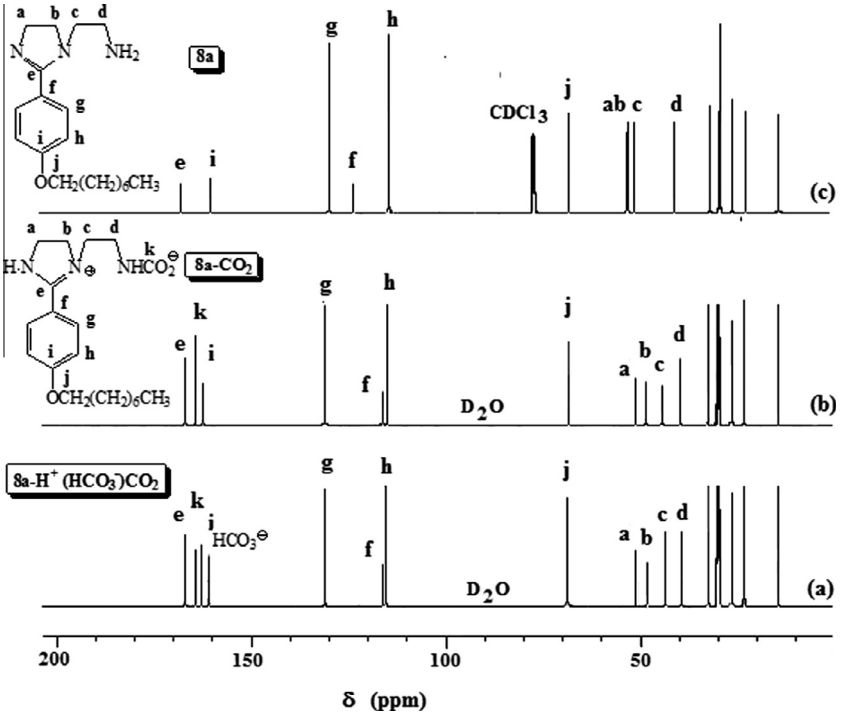

Fig. 12. ^{13}C NMR spectra of (**a**) **8a**-$H^+(HCO_3^-)CO_2$ (in D_2O using dioxin as external standard), (**b**) **8a**-CO_2 (in D_2O) and (**c**) **8a** (in $CDCl_3$, using TMS as internal standard).

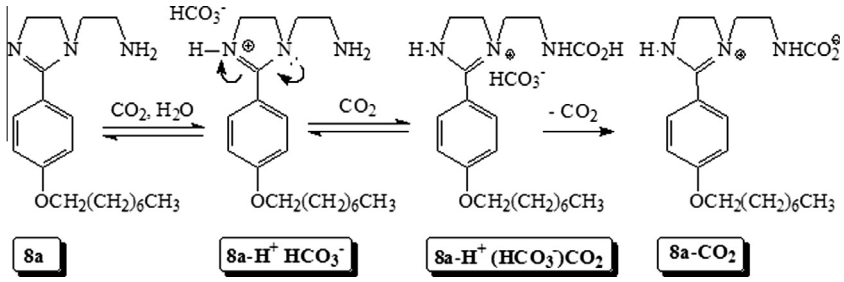

Fig. 13. Reactions of imidazoline **8a** with aqueous CO_2.

equivalent of C. Note that **8c** and **9c** having hydrophobe equivalent to 23 CC bonds outperformed all other imidazolines considered in the current work (Tables 3–5).

Finally, an attempt was made to understand the chemical behavior of the imidazolines in aqueous CO_2. To a mixture of **8a** (65 mg) in D_2O (0.8 cm^3) was passed CO_2 at 40 °C for 5 min. The ^{13}C NMR spectrum revealed the presence of four signals at the chemical shifts of 161.0, 163.0, 164.4 and 167.3 ppm, assigned to the carbons marked as HCO_3^-, **i**, **k**, and **e**, respectively (Fig. 12). The assignment of HCO_3^- was based on literature [10]. The presence of carbon marked '**k**' signal at 164.4 ppm was assigned to the carbamate motif [NHC(=O)O^-]; the absence of any signal at ≈174 ppm precluded the presence of amide motif ([NHC(=O)C—] which would have been generated by hydrolysis of the imidazoline motifs [32]. The reaction in the presence of CO_2 is presented in Fig. 13. Imidazoline **8a** is expected to give the bicarbonate salt **8a**-H^+ HCO_3^- as a result of protonation of the amidine motif; the reaction of the primary amine group (NH_2) would lead to the carbamic acid [12]. In a similar experiment carried out in H_2O, after passing CO_2 followed by removal of the solvent at room temperature the residue was dried under vacuum. The IR spectrum of the residue revealed the absence of any peak around 1640 cm^{-1} thereby asserting that the hydrolysis of the amidine motifs to the amide group did not happen; the presence of peak at 1610 cm^{-1} indicated the presence of protonated amidine [C=N—H^+] [9]. The ^{13}C NMR spectrum of the residue interestingly revealed the absence of HCO_3^- carbon signal; it showed the presence of three carbon signals at 162.5, 164.3 and 167.2 ppm attributed to the carbons marked **i**, **k** and **e** of **8a**-CO_2 (Fig. 12). The spectral analyses thus revealed the formation of bicarbonate salt **8a** followed by bicarbonate/carbamic acid **8a**-$H^+(HCO_3^-)CO_2$ in an aqueous solution. However, in the absence of water, carbonic acid was lost in the form of CO_2/H_2O to give the zwitterionic carbamate **8a**-CO_2 (Fig. 12). To the best of our knowledge, the details chemical reactions of an imidazoline in aqueous CO_2 were studied for the first time. The findings cannot shed any light on how does the imidazolines demonstrate powerful inhibition ability; however, it opens up a new avenue in designing more effective corrosion inhibitors bearing electron-rich amidine motifs.

5. Conclusions

A novel series of imidazolines having an electron-rich aromatic ring embedded in between the heterocycle and the hydrophobic alkyl chains of C_8, C_{12} and C_{18} and two kinds of *N*-pendants – CH_2-NH_2 and $(CH_2CH_2NH)_2CH_2CH_2NH_2$ – have been synthesized. As such, the imidazolines have provided an opportunity to investigate the dependence of the corrosion inhibition efficacy on the *N*-pendants, aromatic ring and hydrophobic alkyl tails. The inhibition efficiencies of imidazolines in CO_2-saturated 0.5 M NaCl at 40 °C increased with the increase in the alkyl chain lengths; imidazolines **8c** and **9c** both having C_{18} alkyl chain achieved IEs over 98% at an inhibitor concentration of 100 ppm. The *N*-pendant of $(CH_2CH_2$-$NH)_2CH_2CH_2NH_2$ was found to impart no significant advantage over its shorter counterpart containing a single nitrogen. The current work showed the beneficial role played by the aromatic ring in conjugation with the N=C—N motifs of the imidazolines.

The compounds acted mainly as anodic inhibitors, with ΔG^o_{ads} values indicative of chemisorption and XPS results ascertained the formation of an adsorbed protective film in CO_2-saturated 0.5 M NaCl. The adsorption process of the imidazolines was found to obey the Langmuir adsorption isotherm. The surface coverage data and CMC values demonstrated that the inhibitor molecules have a greater tendency to undergo adsorption on to the metal surface than to micellize. In autoclave tests, under high CO_2 pressure (10 bar) and temperature of (120 °C) the imidazolines **8b**,**c** and **9b**,**c** all performed considerably better as compared to two commercial inhibitors tested for this purpose. The interesting findings from the current work would indeed be helpful in designing better imidazolines incorporating electron-rich aromatic group in conjugation to the N=C—N motifs.

Acknowledgements

Facilities provided by King Fahd University of Petroleum and Minerals and financial assistance by King Abdulaziz City of Science and Technology (KACST) (under the Grant: AR-26-26) and Deanship of Scientific Research, KFUPM (Startup Grant: IN121036) are gratefully acknowledged.

Appendix A. Supplementary material

Supplementary data associated with this article can be found, in the online version, at http://dx.doi.org/10.1016/j.corsci.2014.09.014.

References

[1] V. Jovancicevic, S. Ramachandran, P. Prince, Inhibition of carbon dioxide corrosion of mild steel by imidazolines and their precursors, Corrosion 55 (1999) 449–455.
[2] X. Liu, S. Chen, H. Ma, G. Liu, L. Shen, Protection of iron corrosion by stearic acid and stearic imidazoline self-assembled monolayers, Appl. Surf. Sci. 253 (2006) 814–820.
[3] X. Liu, P.C. Okafor, Y.G. Zheng, The inhibition of CO_2 corrosion of N80 mild steel in single liquid phase and liquid/particle two-phase flow by aminoethyl imidazoline derivatives, Corros. Sci. 51 (2009) 744–751.
[4] P.C. Okafor, X. Liu, Y.G. Zheng, Corrosion inhibition of mild steel by ethylamino imidazoline derivative in CO_2-saturated solution, Corros. Sci. 51 (2009) 761–768.
[5] F. Farelas, A. Ramirez, Carbon dioxide corrosion inhibition of carbon steels through bis-imidazoline and imidazoline compounds studied by EIS, Int. J. Electrochem. Sci. 5 (2010) 797–814.
[6] M.W.S. Jawich, G.A. Oweimreen, S.A. Ali, Heptadecyl-tailed mono- and bis-imidazolines: a study of the newly synthesized compounds on the inhibition of mild steel corrosion in a carbon dioxide-saturated saline medium, Corros. Sci. 65 (2012) 104–112.
[7] S. Nesic, Key issues related to modelling of internal corrosion of oil and gas pipelines – a review, Corros. Sci. 49 (2007) 4308–4338.

[8] P.A. Koutentis, M. Koyioni, S.S. Michaelidou, Synthesis of [(4-Chloro-5H-1,2,3-dithiazol-5-ylidene)amino]azines, Molecules 16 (2011) 8992–9002.
[9] W. Qiao, Z. Zheng, Q. Shi, Synthesis and properties of a series of CO_2 switchable surfactants with imidazoline group, J. Surfact. Deterg. 15 (2012) 533–539.
[10] D.J. Heldebrant, P.G. Jessop, C.A. Thomas, C.A. Eckert, C.L. Liotta, The reaction of 1,8-diazabicyclo[5.4.0]undec-7-ene (DBU) with carbon dioxide, J. Org. Chem. 70 (2005) 5335–5338.
[11] N. Ramachandran, A. Aboudheir, R. Idem, P. Tontiwachwuthikul, Kinetics of the absorption of CO_2 into mixed aqueous loaded solutions of monoethanolamine and methyldiethanolamine, Ind. Eng. Chem. Res. 45 (2006) 2608–2616.
[12] P.N. Sutar, A. Jha, P.D. Vaidya, E.Y. Kenig, Secondary amines for CO_2 capture: a kinetic investigation using N-ethylmonoethanolamine, Chem. Eng. J. 207–208 (2012) 718–724.
[13] X. Jiang, Y.G. Zheng, D.R. Qu, W. Ke, Effect of calcium ions on pitting corrosion and inhibition performance in CO_2 corrosion of N80 steel, Corros. Sci. 48 (2006) 3091–3108.
[14] G. Zhang, C. Chen, M. Lu, C. Chai, Y. Wu, Evaluation of inhibition efficiency of an imidazoline derivative in CO_2-containing aqueous solution, Mater. Chem. Phys. 105 (2007) 331–340.
[15] U. Lotz, L. Van Bodegom, C. Ouwehand, The effect of type of oil or gas condensate on carbonic acid corrosion, Corrosion 47 (1991) 635–644.
[16] F.F. Eliyan, A. Alfantazi, On the theory of CO_2 corrosion reactions – Investigating their interrelation with the corrosion products and API-X100 steel microstructure, Corros. Sci. 85 (2014) 380–393.
[17] Q.Y. Liu, L.J. Mao, S.W. Zhou, Effects of chloride content on CO_2 corrosion of carbon steel in simulated oil and gas well environments, Corros. Sci. 84 (2014) 165–171.
[18] K. Chokshi, W. Sun, S. Nesic, Iron carbonate scale growth and the effect of inhibition in CO_2 corrosion of mild steel, in: NACE International Corrosion Conference & Expo, Paper #05285, 2005.
[19] J. Han, D. Young, H. Colijn, A. Tripathi, S. Nesic, Chemistry and structure of the passive film on mild steel in CO_2 corrosion environments, Ind. Eng. Chem. Res. 48 (2009) 6296–6302.
[20] F. Farelas, M. Galicia, B. Brown, N. Nesic, H. Castaneda, Evolution of dissolution processes at the interface of carbon steel corroding in a CO_2 environment studied by EIS, Corros. Sci. 52 (2010) 509–517.
[21] F. Bentiss, M. Triasnel, H. Vezin, M. Lagrenee, Linear resistance model of the inhibition mechanism of steel in HCl by triazole and oxadiazole derivatives: structure–activity correlations, Corros. Sci. 45 (2003) 371–380.
[22] A. Edwards, C. Osborne, S. Webster, D. Klenerman, M. Joseph, P. Ostovar, M. Doyle, Mechanistic studies of the corrosion inhibitor oleic imidazoline, Corros. Sci. 36 (1994) 315–325.
[23] S. Ramachandran, B.L. Tsai, M. Blanco, H. Chen, Y. Tang, W.A. Goddard III, The SAM mechanism for corrosion inhibition of iron by imidazolines, Langmuir 12 (1996) 6419–6428.
[24] X. Zhang, F. Wang, Y. He, Y. Du, Study of the inhibition mechanism of imidazoline amide on CO_2 corrosion of Armco iron, Corros. Sci. 43 (2001) 1417–1431.
[25] D. Wang, S. Yong, M. Wang, H. Xiao, Z. Chen, Theoretical and experimental studies of structure and inhibition efficiency of imidazoline derivatives, Corros. Sci. 41 (1999) 1911–1919.
[26] A.J. Szyprowski, Hydrogen sulphide corrosion of steel – mechanism of action of imidazoline inhibitors, in: Proceeding of the Eighth European Symposium on Corrosion Inhibitor (8SEIC) Univ. Ferrara, 1995, pp. 1229–1238.
[27] G. McIntire, J. Lippert, J. Yudelson, The effect of dissolved CO_2 and O_2 on the corrosion of iron, Corrosion 46 (1990) 91–95.
[28] S. Nesic, K.L.J. Lee, A mechanistic model for carbon dioxide corrosion of mild steel in the presence of protective iron carbonate films-part 3: film growth model, Corrosion 59 (2003) 616–627.
[29] M.A.J. Mazumder, H.A. Al-Muallem, M. Faiz, S.A. Ali, Design and synthesis of a novel class of inhibitors for mild steel corrosion in acidic and carbon dioxide-saturated saline media, Corros. Sci. 87 (2014) 187–198.
[30] H.-J. Butt, K. Graf, M. Kappl, Physics and Chemistry of Interfaces, Wiley-VCH, Weinheim, 2003. pp. 253.
[31] Y. Wu, P.R. Herrington, Thermal reactions of fatty acids with diethylene triamine, J. Am. Oil Chem. Soc. 74 (1997) 61–64.
[32] Y. Duda, R.G. Rueda, M. Galicia, H.I. Beltran, L.S.Z. Rivera, Corrosion inhibitors: design, performance, and computer simulations, J. Phys. Chem. B 109 (2005) 22674–22684.
[33] A. Marxer, Imidazole Urea and Amido Compounds, US Patent 4,420,619, 1983.
[34] W. Durnie, R. De Marco, A. Jefferson, B. Kinsella, Development of a structure–activity relationship for oil field corrosion inhibitors, J. Electrochem. Soc. 146 (1999) 1751–1756.
[35] S. Nesic, G.T. Solvi, J. Enerhaug, Comparison of the rotating cylinder and pipe flow tests for flow-sensitive carbon dioxide corrosion, Corrosion 10 (1995) 51773–51787.
[36] S.A. Ali, M.T. Saeed, S.U. Rahman, The isoxazolidines: a new class of corrosion inhibitors of mild steel in acidic medium, Corros. Sci. 45 (2003) 253–266.
[37] A.N. Frumkin, Die Kapillarkurve der höheren Fettsäuren und die Zustandsgleichung der Oberflächenschicht, Z. Phys. Chem. 116 (1925) 466–484.
[38] J.O'M. Bockris, S.U.M. Khan, Surface Electrochemistry: A Molecular Level Approach, Plenum press, New York and London, 1993.
[39] S.A. Ali, H.A. Al-Muallem, M.T. Saeed, S.U. Rahman, Hydrophobic-tailed bicycloisoxazolidines: a comparative study of the newly synthesized compounds on the inhibition of mild steel corrosion in hydrochloric and sulfuric acid media, Corros. Sci. 50 (2008) 664–675.
[40] S.Z. Duan, Y.L. Tao, Interface Chemistry, Higher Education Press, Beijing, 1990. pp. 124–126.
[41] F. Bentiss, M. Triasnel, M. Lagrenee, The substituted 1,3,4-oxadiazoles: a new class of corrosion inhibitors of mild steel in acidic media, Corros. Sci. 42 (2000) 127–146.
[42] S. Kertit, B. Hammouti, Corrosion inhibition of iron in 1 M HCl by 1-phenyl-5-mercapto-1,2,3,4-tetrazole, Appl. Surf. Sci. 93 (1996) 59–66.
[43] W. Jia, A study on the impedance responses of inhibitor desorption, Chin. J. Oceanol. Limnol. 16 (1998) 54–59.
[44] B.I. Podlovchenko, B.B. Damaskin, Possible demarcation of adsorption isotherms based on repulsive interaction and surface inhomogeneity, Elektrokhimiya 8 (1972) 297.
[45] A.E. Stoyanova, E.I. Sokolova, S.N. Raicheva, The inhibition of mild steel corrosion in 1 M HCl in the presence of linear and cyclic thiocarbamides – effect of concentration and temperature of the corrosion medium on their protective action, Corros. Sci. 39 (1997) 1595–1604.
[46] D. Bajpai, V.K. Tyagi, Fatty imidazolines: chemistry, synthesis, properties and their industrial application, J. Oleo. Sci. 55 (7) (2006) 319–329.
[47] W. Wang, M.L. Free, D. Horsup, Prediction and measurement of corrosion inhibition of mild steel by imidazolines in brine solutions, Metall. Mater. Trans. B 36 (2005) 335–341.
[48] K. Esumi, M. Ueno, Structure Performance Relationships in Surfactants, Marcel Dekker Press, 2003.
[49] O. Olivares-Xometl, N.V. Likhanova, M.A. Domínguez-Aguilar, J.M. Hallen, L.S. Zamudio, E. Arce, Surface analysis of inhibitor films formed by imidazolines and amides on mild steel in an acidic environment, Appl. Surf. Sci. 252 (2006) 2139–2152.
[50] M. Tourabi, K. Nohair, M. Traisnel, C. Jama, F. Bentiss, Electrochemical and XPS studies of the corrosion inhibition of carbon steel in hydrochloric acid pickling solutions by 3,5-bis(2-thienylmethyl)-4-amino-1,2,4-triazole, Corros. Sci. 75 (2013) 123–133.